Ion distribution functions and transport properties in collision-free auroral ionosphere under arbitrary electric fields

Filamentary space-charge aurorae bring about cylindrical structures symmetric to local geomagnetic field lines in auroral ionosphere. It produces arbitrary structured electric fields. Developed from *Ma & St.-Maurice* (2008, J. Geophys. Res., 113, A05312), this paper studies collision-free ion distributions and related transport properties by numerically solving the Boltzmann-Vlasov equation under this kind of electric field conditions in auroral ionosphere. various shapes of Non-Maxwellian ion velocity distributions (e.g., tear-drop, core-halo, ear-donut, etc.) and associated transport properties are obtained. The results are applicable to account for ongoing and future high-resolution observations.

1 Introduction

In local thermal equilibrium, the ion distribution function is described by a Maxwellian distribution. However, in the solar-terrestrial system, numerous non-Maxwellian distributions have been found with non-equilibrium characteristics such as beams, temperature or pitch-angle anisotropies. For example, the SOHO spacecraft measured the distribution function of the coronal base and the extended solar-wind acceleration region between 2 and 10 solar radii. Coupled with interplanetary particle measurements going back several decades, the observations strongly suggest that collisionless particles exhibit non-Maxwellian velocity distributions with anisotropic ion temperatures and differential outflows (*Cranmer* 2002). Another example of large distortions from equilibrium is the Io plasma torus (*Steffl* 2005). The tidal heating of Io's interior produces volcanos which expel neutrals (mostly O and S atoms) outward. Through electron impact and charge exchange reactions, the neutrals convert to ions (very intense emissions are seen for O^+, O^{2+}, S^+, S^{2+}, and S^{3+}). Voyager observations demonstrate that at 65 km/s the S^+ velocity distribution has a peak and that of O^+ has a sharp shoulder, while other ions could be more Maxwellian-like (*Banaszkiewicz & Ip* 1993). For electrons, Voyager and Galileo spacecrafts suggest that they may actually be non-thermal or at least have a non-thermal, high-energy tail (*Frank & Paterson* 2000).

In addition, in both the upstream and downstream regions of the Earth's bow shock, the Interball/Tail-probe satellite detected that the upstream ion population has a ring-like (or, halo) distribution, while in the downstream, the distribution has a hot bell-like core and a flat tail (*Yermolaev et al.* 1997). Specifically on field-aligned beams upstream of the bow shock, Cluster observations reported that: (1) parallel to the magnetic field, the distribution is Maxwellian, and (2) perpendicular to the magnetic field, it has a non-thermal, high-energy tail, bringing about a ratio of $\sim$3 between the perpendicular and parallel temperatures (*Meziane et al.* 2006). Moreover, at altitudes ranging from 1000 km up through one Earth radius and beyond, there is another kind of non-Maxwellian distribution, ion conics (*Yau et al.* 1984). Rocket and satellite measurements showed that ions are concentrated into cones in velocity space under different conditions, and the distribution peaks at specific pitch angles, respectively. Even below 1000 km, many direct observations have also shown the ion velocity distributions to depart from

the Maxwellian shape over wide areas. In particular, the retarding potential analyser onboard AE-C satellite has produced convincing evidence for ion velocity distributions with flat-top shapes compared to Maxwellians (*St-Maurice et al.* 1976). The EISCAT incoherent scatter radar also detected the flat-top-shaped distributions in poleward ion flow bursts in the dayside auroral ionosphere (*Lockwood et al.* 1987). The distributions were observed whenever the ion drift exceeded the neutral thermal speed.

Another type of low-altitude non-Maxwellian ion velocity distribution has been found in high-resolution GEODESIC rocket experiments (*Burchill et al.* 2004). It is crescent-shaped in velocity space with a two-ear pattern, and was found in lower-hybrid (LH) cavities. At 980 km altitude, 12 sequenced images were produced as the payload flew through one cavity, displaying non-thermal distributions of transversely-heated ions (*Bock* 2005). Some of the distributions revealed tails associated with the energization of the ion population (*Knudsen et al.* 2004). Artificial plasma disturbances can also produce non-Maxwellian distributions. For instance, two dedicated burns of the space shuttle engines were implemented over the Millstone Hill incoherent scatter radar (*Bernhardt et al.* 2005). The radar recorded ionospheric density depressions resulting from recombination of the molecular ions with electrons. At the same time, radar spectra revealed unusual signatures that may have been produced by ion ring-beam distributions.

From the above, we can see clearly that non-Maxwellian distributions are frequently present in different regions in geospace. Several possible mechanisms have been proposed for the deviation of the distribution from the Maxwellian equilibrium configuration (*St.-Maurice* & *Schunk* 1979): (1) it can be a consequence of the collisionless nature of the medium, particularly in the presence of large or rapidly varying forces acting on the medium, (2) it can occur when a minor constituent of a gas mixture experiences a force (say, $\mathbf{E} \times \mathbf{B}$ drift, where $\mathbf{E}$ and $\mathbf{B}$ represent electric and magnetic fields, respectively) that differs from the forces acting on the major constituent, (3) it can be the result of ion and neutral species chemistry, producing kinetic energies which are substantially different from thermal energies.

The importance of gaining a deep understanding of ion velocity distributions in the ionosphere cannot be understated. First, this is simply a case of making sense of the observations. For instance, when we observe conics, or horseshoe distributions, it would be highly desirable to understand how they form, and to test the data against particular theories. Secondly, a large departure from an equilibrium Maxwellian distribution goes hand in hand with important modifications to transport properties. For example, conics are very efficient at 'expelling' ionospheric ions into the magnetosphere through a mirror effect. Likewise, a strong temperature anisotropy will modify the vertical transport, and strong skewness will create heat flow, etc. Furthermore, a proper interpretation of ionospheric measurements (satellites, rockets, radars) often depends on a knowledge of the velocity distribution. In the data inversion process of the satellite measurements, for example, *St-Maurice et al.* (1976) found that, if the temperature is above 2000 K, the interpretation can be seriously affected when the normally assumed ion Maxwellian distribution is used. For example, the atomic to ion molecular ion density ratios can be affected by a factor of 2 or more, and for the very high temperature data (> 3000 K) the ion temperature can be underestimated by as much as 2700 K. Similar problems also exist in the spectral analysis of the radar waves scattered incoherently from the ionosphere above 150 km. At these altitudes, the ion-neutral collision frequency is small compared to the ion gyrofrequency. *Raman* (1980) and *Raman et al.* (1981) found that electric fields larger than 45 mV/m could cause a serious underestimation of the electron-ion temperature ratio, sometimes by as much as a factor of 2. This results in an error of several hundred degrees Kelvin in the interpreted electron and ion temperatures. Last but not least, large departures from Maxwellian may play a role in the excitation of plasma micro-instabilities. In the auroral F region, for example, if the perpendicular electric field exceeds $\sim$50 mV/m, the non-Maxwellian distribution may excite short wavelength instabilities of $\sim$10-20 cm (*Ott* & *Farley* 1975; *St.-Maurice* 1978).

As a matter of fact, the auroral ionosphere is permeated by strong electric fields which can be as high as several hundred mV/m. Contrary to those at other latitudes, these electric fields are not produced by neutral wind dynamos, but rather by processes that go back to the solar-wind–magnetosphere–ionosphere (SMI) electrodynamic coupling processes. The electrodynamics in the SMI system is described in great detail by, e.g., *Akasofu* (1977,1981a,b); *Kan* & *Akasofu* (1989); and *Lyon* (2000). The induced large-scale convection electric field in the high-latitude regions provides a fair context for the average flow. However, a multitude of measurements from low-altitude satellites, rockets, radars, and

from optical means have shown that electric field measurements with insufficient temporal resolution can sometimes hide very large fluctuations and sharp transitions over a wide range of spatial and temporal scales.

For example, the S23L1 rocket discloses that, over a short distance around an auroral arc, electric field went down from ∼110 mV/m to ∼20 mV/m. The drop occurred in about 10 s, that is, on a scale of 10 km (*Marklund et al.* 1982). In a more complicated case, the ARCS-4 rocket obtained ionic O^+ and the DC electric field data (*Moore et al.* 1996). At ∼500 km altitudes, the electric field oscillated violently after launch time about 570 s. The oscillations were considered to be related to vortical structures. The perpendicular drift could soar up to 3 km/s, with a velocity shear ∼0.75 m/s per meter or more. At similar altitudes, *Earle et al.* (1989) observed an even more structured event, namely, a change of 180 mV/m over 363 m, corresponding a shear of ∼11 m/s per meter. More strikingly, the authors even recorded a change larger than 200 mV/m over a short distance with a shear of ∼25 m/s per meter.

In addition to arcs, there are several examples of cylindrical structures or "vortices" at high latitudes. Some vortices have large scales (500-1000 km in diameter) and are seen easily by, e.g., radars like SuperDARN. Some of them have been labeled as "quasi-stationary convection vortices", and have been shown to be closely connected to the region-1 field-aligned currents, with a lifetime ∼10-20 min (up to 50 min). The related potential drop is 5-10 kV. The center of the vortex was considered to link with a stable, upward, filament-like, field-aligned current (see, e.g., *Alexeev et al.* 1997; *Huang et al.* 1998). At 400-500 km altitude, smaller vortices have also been observed by rockets. A multi-instrumental measurement campaign involving magnetometer, rocket, and all-sky camera data detected spirals of about 100 km in diameter. These usually rotate clockwise, but sometimes counterclockwise (*Pietrowski et al.* 1999; *Danielides* & *Kozlovsky* 2001). They appear at the poleward boundary of the nightside auroral oval. Afterwards, they form a poleward displaced bulge at the pre-or-post midnight sector. Auroral Turbulence II Rocket data (*Pietrowski et al.* 1999) demonstrated that the electric field could reach up to 1.1 V/m with a shear 4 m/s per meter or more. The peak shear region (about 1 km) was devoid of precipitation. Much smaller scales of cylindrical structures have also been confirmed in the topside ionosphere at 500∼1000 km altitudes. They are called lower-hybrid (LH) cavities. They have scales of tens of meters in width (or chord lengths). The GEODESIC & OEDIPUS-C sounding rockets measured the VLF electric field and the magnetic field (*Bock* 2005), the spatially density-depletion (*Knudsen et al.* 2004), and count images in velocity space (*Bock* 2005). Both the electric and magnetic signals are spikelike, either single-peaked or double-peaked. The electric field gradient can be up to 30 mV/m over a few Debye lengths (several tens of meters).

Undoubtedly, in the auroral ionosphere, the transverse electric fields can become very strong locally, up to ∼1 V/m. The regions are either associated with elongated arcs (Cartesian geometry) or cylindrically symmetric. Shears existing in these regions have been observed to reach up to 25 m/s per meter. There are probably higher shears than that. As the spatial and temporal resolution of the observations is improving, more and more such events should be measured. Once a localized DC electric field $\mathbf{E}$ is established crossed to the ambient magnetic field $\mathbf{B}$, an $\mathbf{E} \times \mathbf{B}$ drift occur inevitably for charged particles. For strong electric fields, the drift speed can reach several km/s. This drift is considerable compared to the normal ion thermal speed and compared to the thermal speed of the neutral gas with which the ions collide. As a result, there can be strong deviations for ions from a thermal (Maxwellian) velocity distributions (*St.-Maurice* & *Schunk* 1979). This is true of both the collisional and collision-free problems. The later applies to time scales shorter than a collision time. Notice that electrons are not influenced due to their much higher thermal speeds (tens of km/s).

Until now, the study of ion velocity distributions in the ionosphere has been done for a uniform electric field in both collisional and collision-free cases. An initial study involving an inhomogeneous electric field in collisional cases has also been completed. In a pioneering study, *Cole* (1971) determined how far the ion distribution can deviate from the equilibrium Maxwellian in a uniform electric field in the collisionless case. He found that the distribution function is determined completely by the characteristics of ion motion, or, precisely, by the energy conservation of ion motion in the electromagnetic field. By considering an initial Maxwellian ion distribution in the absence of the electric field, he obtained an ion velocity distribution which pulsated about the $\mathbf{E} \times \mathbf{B}$ drift. For $E \geq 10$ mV/m, the average ion distribution started to deviate significantly from a Maxwellian. *Schunk* & *Walker* (1972) generalized

Cole's work by including the collisional term. Formally, the collision term is described by the Boltzmann collision integral. By expanding the distribution function using a complete orthonomal polynomial series of the products of Sonine polynomials and spherical tensors, the authors obtained a Maxwellian-weighting, infinite-component solution of the Boltzmann equation. The results were applicable to small distortions from the initial Maxwellian, such as can be found with small electric fields, and/or high ion-neutral collision frequencies. They found that the departure from a Maxwellian was small below 120 km (where the collision frequency is comparable to the ion cyclotron frequency). Above that altitude, the departure was basically the same at all altitudes below 300 km. As with Cole's results, a 10 mV/m electric field was deemed to be strong enough to cause appreciable non-Maxwellian effects. *St-Maurice & Schunk* (1973,1974) expanded *Schunk & Walker*'s work to strong electric fields. They used a simple relaxation model in place of the Boltzmann collision integral. Physically, this model assumes that the target neutral has a velocity $\mathbf{v}_\mathrm{n}$, satisfying a Maxwellian distribution. When an ion with velocity $\mathbf{v}_\mathrm{i}$ collides with the neutral, the particles exchange velocities ($\mathbf{v}_\mathrm{n}$ is replaced by $\mathbf{v}_\mathrm{i}$ and vice versa). The ion takes the neutral's Maxwellian velocity distribution in phase space before regaining momentum and energy from the electromagnetic fields. The neutral subsequently moves with the traded velocity until colliding with other neutrals. The time scales over which the entire ion velocity distribution will change is, not surprisingly, ν_{in}^{-1}, a time long enough for all ions to experience roughly one collision. The authors obtained analytical solutions to the Boltzmann equation for all electric field strengths and collision frequencies. In the small collision regime ($\nu_{in} \ll \Omega_i$), namely, above 150 km, the ion distribution formed a torus for electric fields higher than 40 mV/m. By contrast, in a region close to 120 km ($\nu_{in} \sim \Omega_i$), the distribution was bean-shaped for electric fields of 100 mV/m or more. The departure of the ion distribution from a Maxwellian was confirmed by radar measurements (*Swift* 1975; *Lockwood et al.* 1987) and satellite observations (*St-Maurice et al.*, 1976). In the later, *St-Maurice et al.* (1976) developed a method to scale the analytical results for data analysis purposes, and to retrieve plasma data from the non-Maxwellian distribution in the small collision frequency regime. They used a relaxation model to describe ion-neutral collisions in solving the ion velocity distribution from the Boltzmann equation.

If the electric field is not homogeneous, that is, if there are spatial divergences in $\mathbf{E}$ (and thus shears in the $\mathbf{E} \times \mathbf{B}$ drift), the physical mechanism and mathematical formulations become much more complex than what was presented in the last section in solving the Boltzmann equation. Even the simplest parameter, the ion gyrofrequency Ω_i, changes from $\Omega_i = qB/m_i$ in the homogeneous field to a new definition in the inhomogeneous field. For example, if the first derivative of the field ($\nabla \cdot \mathbf{E} = \mathrm{d}E_x/\mathrm{d}x$) is nonzero, while the second derivative $\left(\mathrm{d}^2E_x/\mathrm{d}x^2\right)$ is zero, *Cole* (1976) showed that the effective gyrofrequency ω satisfies $\omega^2 = \Omega_i^2 + \Omega_i \mathrm{d}(E_x/B)/\mathrm{d}x$. In addition, he found that it is possible to accelerate ions when the gyro-radius is larger than the scale length of the potential well. *Rothwell et al.* (1995) stated that for $\mathrm{d}^2E_x/\mathrm{d}x^2 \neq 0$, there are two criteria about the gradients: $\mathrm{d}\left(E_x/B\right)/\mathrm{d}x \geq \Omega_i$, and, $\mathrm{d}^2\left(E_x/B\right)/\mathrm{d}x^2 \geq 3\omega\Omega_i/(8v_0)$ (where v_0 is the initial velocity). For the first condition, the kinetic theory has to be used instead of either ideal or non-ideal MHD theory; if the second one is satisfied, untrapped ions occur. For a more complicated field, $E_x \sim x\mathrm{e}^{-x^2}$, *Rothwell et al.* (1992) and *Anastasiadis et al.* (2004) showed that particles are either trapped or untrapped in the potential well; and, if the characteristic length of the well is comparable to the gyroradius, stochastic heating can occur depending upon initial conditions of the phase angle $\theta = \arctan(v_{y0}/v_{x0})$ (where v_{x0}, v_{y0} are initial velocity components) and kinetic energy.

In the collision-free regime, *Ganguli et al.* (1988) obtained collision-free ion velocity distributions again following the onset of a perpendicular electric field with a linear divergence. The authors had in mind instability calculations in the presence of shears at high enough altitudes, so that collisions would not affect the velocity distributions for a sufficiently long time. After finding the invariants for the problem, the authors used an arbitrary distribution of this invariant without attempting to relate this distribution to a particular initial or boundary condition. This choice of solution may have been valid for a slowly changing electric field in time. However, the thesis shows that the task of actually linking the collision-free distribution even just to simple initial conditions for a fast change in the electric field can actually be surprisingly non-trivial even when all the invariants of the motion

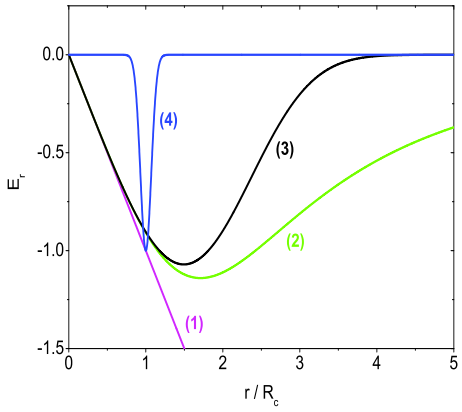

Fig. 1 Arbitrary radial electric field examples which are constant in time: (1) $E_r = -E_c(r/R_c)$; (2) $E_r = -E_c(r/R_c)/[1 + 0.1\,(r/R_c)^3]$; (3) $E_r = -E_c(r/R_c)e^{-0.1(r/R_c)^3}$; and (4) $E_r = -E_c e^{-(r/R_c-1)^2/0.1^2}$.

are known. To our knowledge, there has only been one study of more complicated problems to obtain velocity distributions in the presence of perpendicular inhomogeneous electric fields in the collisional regime. The work was done by *St.-Maurice et al.* (1994). To solve the very complicated Boltzmann equation in the nonhomogeneous electric field, the authors selected a model with a relatively simple electric field varying linearly in space along a particular direction, perpendicular to the magnetic field: $\mathbf{E} = E_0(1 + y/L)\hat{\mathbf{y}}$ in Cartesian geometry (where E_0 is the field at $y = 0$, L the characteristic length, y the ion position). Focusing on the collision-dominated case, the authors found that a phase-average model involving ion characteristics could be used to solve for the ion velocity distribution, and associated transport properties.

The calculations were carried out for a simple relaxation collision model; a similar model had been used in earlier work to get the basic physical description of the velocity distribution for the uniform perpendicular electric field case. By comparison to the uniform case, the new velocity distributions in the F region were crescent-(or horseshoe-) shaped, while retaining their symmetries along the electric field direction (in agreement with the fact that Pedersen currents are weak in the F region). The distortions from the toroidal shape were found to be due to the fact that ions coming from more distant points in space had suffered more acceleration and were therefore more energetic than ions coming from closer locations. The study also established that the inhomogeneity in the field had to be on scales of the order of a few gyroradii in order for the departures from the more familiar toroidal shape to be substantial. To set up the phase-averaging, the model used the phase angle ωt instead of time t in the integration over time. As a result, either the collisionless or collisional velocity distribution could be analytically expressed by a series of Bessel functions. The results showed "horseshoe-shaped" ion distributions. The stronger the electric field is, the more evident the horse-shoe shape becomes. Note that the mean ion drift velocity is different from the $\mathbf{E} \times \mathbf{B}$ drift velocity in the plots. This was shown to be the result of the shears in the mean flow. In spite of the different geometry, the theoretical results offer some similarities with recent rocket data of LH cavities (*Burchill et al.* 2004; *Knudsen et al.* 2004; *Bock* 2005).

As discussed above, ionospheric plasmas have two types of geometries of interest: auroral arcs and vortices of various scales. These geometries can be described by a Cartesian frame (x, y, z) and a cylindrical frame (r, ϕ, z). Considering most previous work was done in the x, y, z-frame, but observations have shown many instances of cylindrical charge/electric field arrangements in the auroral ionosphere, we thus turn our attention to the ion velocity distributions that one should expect in the auroral plasma in a cylindrical geometry. It deserves to repeat here that, on larger scales, convection vortices (1000-3000

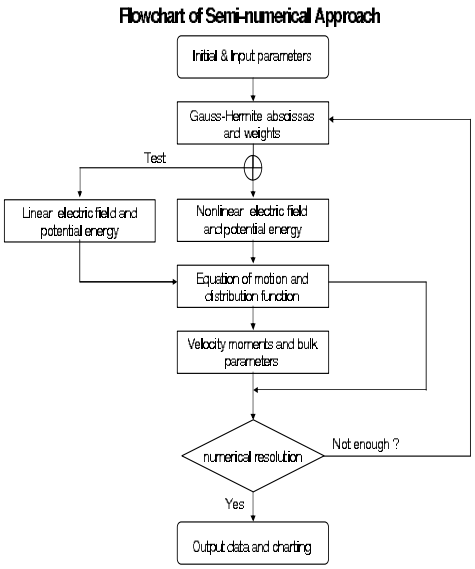

Fig. 2 Flowchart of the semi-numerical approach used for generalized nonlinear electric fields which are constant in time.

km in size) have been reported and studied by a number of authors [e.g., *Vogelsang et al.* (1993); *Huang et al.* (1998)]; smaller cylindrical regions are also known to exist, for example in auroral rays (*Baranoski et al.* 2003). The smallest ionospheric cylindrical structures that we are aware of can be as small as 10 to 20 m, and have been described as lower hybrid cavities (*Schuck et al.* 2003). From a review of similar problems to a certain extent studied in other types of plasmas (fusion plasma, for example) by, e.g., *Vandenplas & Gould* (1964), *Whealton & Woo* (1971), *Roig & Schoutens* (1986), *Date & Shimozuma* (2001), and *Takahashi et al.* (2004), we realize that the complexity of the calculation in a cylindrical geometry requires that we approach the cylindrical geometry through a series of incremental steps, so as to be able to understand the physics and develop suitable approaches, and, based on which to solve more realistic problems.

In the first step, *Ma & St.-Maurice* (2008) (hereafter referred as Paper 1) dealt with the most basic problem we were able to solve towards the goal to gain important insights into the more complicated situations, while still obtaining complete analytical solutions: we tackled a situation for which the strength of the ambient electric field is proportional to the radius of the cylinder, but is constant in time. We focused on ions that are well inside the cylinder, thereby neglecting radial edge effects and features associated with the decaying field outside the cylinder. We assumed that the cylinder has negative space charges due to electron precipitation, and these electrons need not exceed the ambient density by more than one charge in 10^5. We solved a collision-free problem, with an underlying physical model that a time scale considered is much shorter than the ion gyroperiod. The ambient electrons, with their small gyroradii and large thermal speeds, can be assumed to simply remain Maxwellian while experiencing $\mathbf{E} \times \mathbf{B}$ drift in response to the radially linear $\mathbf{E}$ produced by the uniform space charges. In that initial work, $\mathbf{E}$-field is assumed to be maintained, irrespective of the ion response. The solutions thus obtained have proved useful for more realistic applications such as in a collisional case (*Ma & St.-Maurice* 2014): Ion-neutral collisions have effects on the ion velocity distribution and its related transport properties under cylindrically symmetrical conditions associated with the introduction of a radial electric field which is proportional to radius. By using a relaxation collision model for substituting the Boltzmann collision integral in the Boltzmann equation, we showed that collisions drive the velocity distribution to a horseshoe shape after a few collision times. This feature extends to all radial positions as long as the electric field increases linearly with radius. If the electric field is introduced suddenly, there is a transition from the collision-free pulsating Maxwellian obtained in Paper 1 to the horseshoe

shape on a time scale of a few collision times. The transport properties evolve in a similar fashion, from an oscillating to a non-oscillating behavior over the same time interval.

Owing to the fact that (1) understanding velocity distributions is very important if we are to understand the small-scale physics and the fundamental measurements made by incoherent scatter radars, rockets, and satellites; (2) in physics, knowing what creates the distribution will tell us about the forces that act at any given instant; and (3) in experiments, we should rely on a known velocity distribution with the knowledge that we have a good command of what we measure, e.g., the temperature, compositions, etc., we expand our knowledge in this paper beyond the early work, in order to see how ions respond to large electric fields in the ionosphere with arbitrary shears in the cylindrical geometry under collision-free conditions (applicable to altitudes higher than 500 km). Specifically, we study how the interplay between the auroral ionospheric plasma and the $\mathbf{E}\times\mathbf{B}$ drift affects the ion velocity distribution in the presence of arbitrary transverse electric fields that change radially. The situation is now more complicated because the space-charge cylinder no longer has an infinite radius. This forces the electric field strength to change arbitrarily in space, and the ion orbits are no longer locked in phase, except, maybe, in the extreme inner part of the cylinder. Elsewhere, ions that start at different radial distances will feel different oscillation frequencies. The layout of the paper is as follows. Section 2 generalizes Paper 1's analytical work by introducing a semi-numerical "backward ray-tracking" approach. Section 3 gives the algebra to calculate various shapes of ion velocity distribution functions, as well as transport properties at the same time. Section 4 presents simulation results under different electric field models which vary nonlinearly with radius. Finally, Section 5 summarizes the work and discusses some important extensions based on what we obtained. Throughout the paper, SI units are used.

2 Generalized electric field model and equations of motion

For an arbitrary electric field structure, the cylindrically symmetric space charges are no longer extending to infinity but localized to form a cylinder in real space. Various situations are possible for the electric field strength as a function of radial distance. These can, for instance, be a negative charge density peaking near the edge of the cylinder, or, fast or slow changing profile crossing the edge, etc. Different charge density distributions produce different space-charge electric fields. The general problem is simply described by

$$\mathbf{E} = E_r\hat{\mathbf{r}} = E_c \cdot f\left(r\right)\hat{\mathbf{r}} \tag{1}$$

in which E_r denotes a radial electric field strength with a characteristic value E_c at a characteristic radius R_c, $f(r)$ is constant in time, but an arbitrary radial function versus r/R_c, defined as $f(r) = E_r/E_c$. Fig.1 gives several examples of arbitrary $f(r)$ profiles that will be considered in this paper. For comparison, the linear electric field used by *Ma & St.-Maurice* (2008,2014) is also shown.

As discussed in Paper 1, the ion velocity distribution is evidentally affected by the electrostatic potential energy P. The change in P as an ion moves from r_0 to r is given by

$$\left.\begin{array}{l} P_{rr_0} = P_r - P_{r_0} = e[\varphi(r) - \varphi(r_0)] = \\ = e\int_{r_0}^{r}\mathbf{E}\cdot\mathrm{d}\mathbf{r} = e\int_{r_0}^{r}E_r\mathrm{d}r = eE_c\int_{r_0}^{r}f(r)\mathrm{d}r \end{array}\right\} \tag{2}$$

For an electric field proportional to radius as supposed in Paper 1, $f(r) = r/R_c$, we have obtained

$$\left.\begin{array}{l} P_{rr_0} = \frac{1}{2}eE_cR_c\left[\left(\frac{r}{R_c}\right)^2 - \left(\frac{r_0}{R_c}\right)^2\right] = \\ = \frac{1}{2}m_i\frac{E_c}{B}R_c\Omega_i\left[\left(\frac{r}{R_c}\right)^2 - \left(\frac{r_0}{R_c}\right)^2\right] \end{array}\right\} \tag{3}$$

For electric fields unproportional to radius, however, the potential energy may not take such a simple analytical shape. Furthermore, even even for simple cases [e.g., $E_r = E_c(R_c/r)$], we still do not know how to connect r to r_0 and then to determine the potential energy. The problem gets worse for the "exponential" or the "cube" electric field structures introduced in Fig.1. However, this relation can be provided by solving the equation of motion analytically or numerically.

The equation of motion in an arbitrary radial electric field has the form [e.g., Eq.(5) in Paper 1]

$$\left.\begin{array}{l} \frac{\mathrm{d}r}{\mathrm{d}t} = v_r \\ \frac{\mathrm{d}v_r}{\mathrm{d}t} = -\left(\frac{\Omega_i}{2}\right)^2 r - \frac{E_c}{B}\Omega_i \cdot f(r) + \frac{K^2}{m_i^2 r^3} \\ \frac{\mathrm{d}\phi}{\mathrm{d}t} = \omega = \frac{K}{m_i r^2} - \frac{1}{2}\Omega_i \end{array}\right\} \tag{4}$$

In this set of differential equations of motion, the exact relation between the effective gyro-frequency ω and the magnetic gyro-frequency Ω_i is unknown. We therefore choose Ω_i as the timescale parameter in the numerical calculations. Using the "backward ray-tracing" technique, Eq.(4) becomes

$$\left.\begin{array}{lcl} \frac{\mathrm{d}r_0}{\mathrm{d}t} & = & -\frac{2\pi}{R_c\Omega_i} v_{r0} \\ \frac{\mathrm{d}v_{r0}}{\mathrm{d}t} & = & \frac{2\pi}{R_c\Omega_i}\left[\left(\frac{R_c\Omega_i}{2}\right)^2 r_0 + \frac{E_c}{B}R_c\Omega_i \cdot f(r) - \frac{c_k^2}{r_0^3}\right] \\ v_{\phi 0} & = & \frac{r}{r_0}v_\phi + \frac{1}{2}R_c\Omega_i\left(\frac{r^2}{r_0} - r_0\right) \\ c_k & = & r^2\left(\frac{v_\phi}{r} + \frac{1}{2}R_c\Omega_i\right) \end{array}\right\} \tag{5}$$

where all parameters of position, speed, or time are dimensionless in units of R_c, v_T, or, $2\pi/\Omega_i$, respectively. Note that $\{r, v_r, v_\phi\}$ are input parameters, $\{r_0, v_{r0}, v_{\phi 0}\}$ are outputs, and $r_0 = r_0(r, v_r, v_\phi)$, $v_{r0} = v_{r0}(r, v_r, v_\phi)$, $v_{\phi 0} = v_{\phi 0}(r, v_r, v_\phi)$.

3 Numerical calculations for distribution function and bulk properties

In the absence of collisions, Paper 1 tells us that the ion distribution function $f_i[\mathbf{r}(t), \mathbf{v}(t)]$ in phase space at any time t is determined by the initial distribution function $f_i(\mathbf{r}_0, \mathbf{v}_0)$ at $t = 0$:

$$f_i[\mathbf{r}(t), \mathbf{v}(t), t] = f_i(\mathbf{r}_0, \mathbf{v}_0, 0) = f_0 = \frac{n_0}{\pi} e^{-(v_{r0}^2 + v_{\phi 0}^2)} \tag{6}$$

Here, we still assume the initial ion distribution function to be Maxwellian. Using Eq.(2), we immediately find that

$$\left.\begin{array}{l} f_i[\mathbf{r}(t), \mathbf{v}(t), t] = \frac{n_0}{\pi} e^{-[v_r^2 + v_\phi^2 + (P_r - P_{r_0})]} = \\ = \frac{n_0}{\pi} e^{-\left[v_r^2 + v_\phi^2 - 2\frac{E_c}{B}R_c\Omega_i \int_r^{r_0} f(r)\mathrm{d}r\right]} \end{array}\right\} \tag{7}$$

in which P is dimensionless with $mv_T^2/2$, and $r_0 = r_0(r, v_r, v_\phi)$ is numerically calculated from Eq.(5). Using f_i, the following velocity moments can be expressed from the definitions:

$$\left.\begin{array}{ll} n_i = \int f_i \mathrm{d}\mathbf{v} & \\ \langle v_r \rangle = \frac{1}{n_i}\int v_r f_i \mathrm{d}\mathbf{v}\ , & \langle v_\phi \rangle = \frac{1}{n_i}\int v_\phi f_i \mathrm{d}\mathbf{v} \\ \langle v_r^2 \rangle = \frac{1}{n_i}\int v_r^2 f_i \mathrm{d}\mathbf{v}\ , & \langle v_\phi^2 \rangle = \frac{1}{n_i}\int v_\phi^2 f_i \mathrm{d}\mathbf{v} \\ \langle v_r^3 \rangle = \frac{1}{n_i}\int v_r^3 f_i \mathrm{d}\mathbf{v}\ , & \langle v_\phi^3 \rangle = \frac{1}{n_i}\int v_\phi^3 f_i \mathrm{d}\mathbf{v} \end{array}\right\} \tag{8}$$

The moments are obtained numerically by applying the Gauss-Hermite weight integrations. From there, the bulk parameters can be calculated as follows:

$$\left.\begin{array}{l} v_{\mathrm{d}r} = \langle v_r \rangle\ , \quad v_{\mathrm{d}\phi} = \langle v_\phi \rangle \\ T_r = 2\left(\langle v_r^2 \rangle - \langle v_r \rangle^2\right)\ , \quad T_\phi = 2\left(\langle v_\phi^2 \rangle - \langle v_\phi \rangle^2\right) \\ p_{rr} = n_i T_r\ , \quad p_{\phi\phi} = n_i T_\phi \\ q_r = \langle v_r^3 \rangle - \langle v_r \rangle^3 - \frac{3}{2}\langle v_r \rangle \cdot T_r\ , \\ q_\phi = \langle v_\phi^3 \rangle - \langle v_\phi \rangle^3 - \frac{3}{2}\langle v_\phi \rangle \cdot T_\phi \end{array}\right\} \tag{9}$$

The validity of the semi-numerical code was checked against analytical solutions from Paper 1 under the $E \propto r$ case at $r = R_c$ and the time is at $t/T = 3/4$ where $T = 2\pi/\omega$ and ω is the effective

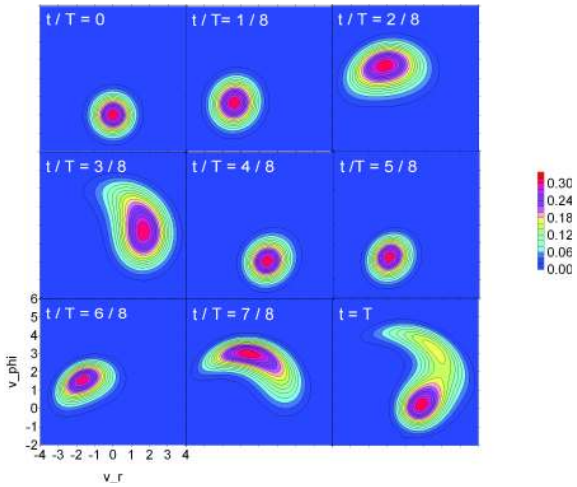

Fig. 3 Ion velocity distribution function versus time at $r = R_c$ and at $E_c/B = 2$ for $E_r = -E_c(r/R_c)/\left[1+0.1\,(r/R_c)^3\right]$. In all panels, $T = 2\pi/\Omega_i$.

gyrofrequency defined in Paper 1. The error is within 9×10^{-6}. In addition, we also checked the fit of the bulk parameters between the analytical and numerical calculations. Except that in $t \in (0.2 \sim 0.3)$ and $t \in (0.7 \sim 0.8)$ the heat flow deviates from zero up to 0.0839, all the other properties have zero deviations.

We mention here that Fig.1 should cover a reasonable range of ionospheric possibilities at least qualitatively. In addition to the simple Curve 1 case already discussed in Paper 1, Fig.1 shows three typical types of radial electric field structures which are not proportional to the radial position:

(1) Curve 2: $E_r = -E_c(r/R_c)/[1+0.1\,(r/R_c)^3]$. Within $r = R_c$, E_r is proportional to r; outside $r = R_c$, E_r decreases to zero slowly relative to Curve 3.

(2) Curve 3: $E_r = -E_c(r/R_c)e^{-0.1(r/R_c)^3}$. Within $r = R_c$, E_r is proportional to r; outside $r = R_c$, E_r decreases to zero quickly relative to Curve 2.

(3) Curve 4: $E_r = -E_c e^{-(r/R_c-1)^2/0.1^2}$. At an arbitrary position in space ($r = R_c$ is taken as an example), there is an electric field jump.

We thus calculate the typical velocity distributions and associated transport properties under these different electric field variations in space. A flow chart describing the computer procedure used to solve the problem is given in Fig.2.

4 Ion distribution functions in different cases

In three more realistic, spatially inhomogeneous electric field structures, Curve 2-4, in Fig.1 than Curve 1, we reply on the generalized semi-numerical "backward ray-tracking" code to calculate the ion velocity distributions and bulk parameters. The results are as follows.

4.1 Case 1: Slowly disappearing E versus r after maximum

Fig.3 uses nine panels to show the evolution of the ion O^+ distribution function in velocity space from $t = 0$ to the same length of time in a magnetic gyro-period [$T = 2\pi/\Omega_i = 2\pi m/(eB)$]. Notice that this gyro-period is that of ions under zero electric field. So, it is not the actual "gyro-period" of ions gyrating under the electric field 2 in Fig.1.

However, there may or may not be such a "gyro-period" shared by all particles in motion. In a field which does not change linearly along the radial direction, ions are not in phase. This is the difference from what Paper 1 describes: the motion of all ions are in phase under linear electric fields. This means in the present case that ions with different initial conditions move in different characteristics in space

with their respective gyro-frequencies. Thus, when we use the phrase "guiding center (GC)" in the following text, we do not refer to the center of the distribution function for all ions as a whole, but only to the so called "center" of the dominant part of the distribution functions (maybe several parts) in velocity space.

Fig.3 is plotted with two input parameters: the radial position is at $r = R_c$ and $E_c/B = 2$. Though the electric field is nonlinear in the radial direction, we notice that it contains a linear component: if r is small, the field turns out to be a linear electric field, meaning the charge density is still uniform close to the center of the space charge cylinder as discussed in Paper 1. Thus, we guess that the ion velocity distribution at $r = R_c$, a radial position not very far from and not very close to the center, should bring, more or less, the features of the distributions introduced in Paper 1. Let's have a close look at the figure.

Firstly, the figure shows a similar rotation feature as that in Paper 1: the ion distribution function rotates continuously around some center related to the $\mathbf{E} \times \mathbf{B}$ drift on the v_ϕ-axis. The panels at $t/T = 3/8$ and $t = T$ illustrate that the center seems to be located at $v_\phi = 2$. We know from Chapter 2 that the $\mathbf{E} \times \mathbf{B}$ drift is $E_r/B = (E_c/B) \times (r/R_c) = 2$ at $r = R_c$. Secondly, all panels together show roughly a periodic change in sizes of the evolving ion distribution function. At first as in the panel at $t/T = 0$, the area of the distribution is small; then it increases, decreases, and increases, oscillating in time. This is exactly the feature shown in Paper 1 for the evolution of the ion distribution in time. Lastly, the gyration of ions appears to have the same effective gyro-frequency (ω) as that given in Paper 1: there, the value of ω turns out to be $\sim 1.9\Omega_i$ for $E_c/B = 2$. This means during one magnetic gyro-period ($1/\Omega_i$), ions have experienced approximately 2 rotations with the effective gyro-frequency ω. See the nine panels in Fig.3: they roughly have rotated twice from $t = 0$ to $t = T = 2\pi/\Omega_i$.

Though with so many similar features to the case in Paper 1, Fig.3 does tell us obvious differences of ion velocity distributions from that under the linear radial electric field structures. For example, because ions are no longer in phase, the appearance of the distribution function does not keep the original "cake" shape at panel $t/T = 0$ they are evolving from, unlike that in Paper 1. At panel $t/T = 3/8$, the distribution function becomes teardrop-shaped; while at panel $t = T$, it is scattered to such a weird shape that a tail emerges out from the core body. Another related feature different from that in Paper 1 is: both the density and temperature are no longer keeping the same variations; more than that, each of them does not oscillate in the same way from one gyration to the other. For instance, it is impossible to find two panels in Fig.3 which have areas (indicating ion density) or the diameters (indicating ion temperature), respectively, of the same size. Moreover, the so called "GC" speed never reaches twice the $\mathbf{E} \times \mathbf{B}$ drift as obtained in Paper 1. See panel $t/T = 2/8$. The "GC" speed is obviously lower than 4. Unlike the linear field case where ions at larger radius feel stronger electric force to accelerate them inward to higher speeds when deflected into the region of interest by the magnetic field, the nonlinear field we are using is localized and no ions outside several R_c are driven inward. Thus, ions with higher speeds are lacking in the region of interest. Naturally, the bulk speed of all ions is unable to touch the top of the circle delineated by the GC motion in velocity space around the $\mathbf{E} \times \mathbf{B}$ drift shown in Paper 1.

4.2 Case 2: Quickly disappearing E versus r after maximum

If the space charge diffusion outside the region of interest is not as high as in Case 1, the ion velocity distribution function is still determined by the localized electric field structure in the region. Curve 3, on the one hand, is not much different from Curve 2 for small r and is still linear along the radial direction. This means the evolution of the distribution function should still have, more or less, the features given in Paper 1. On the other hand, at larger radius, the electric field falls to zero, just like in Curve 2. Thus, we can predict reasonably that the evolution of the distribution function should have, more or less, the features given in Case 1. See Fig.4 for these similarities.

The nine panels show nearly the same evolving features as Case 1 in the gyration period, the top GC speed, the distribution shapes, etc. The only conspicuous difference lies in the tail shown in the last panel at $t = T$: the ion distribution appears to be larger even in the core and tail parts than that shown in Fig.3. This may be explained by the fact that a narrower space charge boundary brings about a

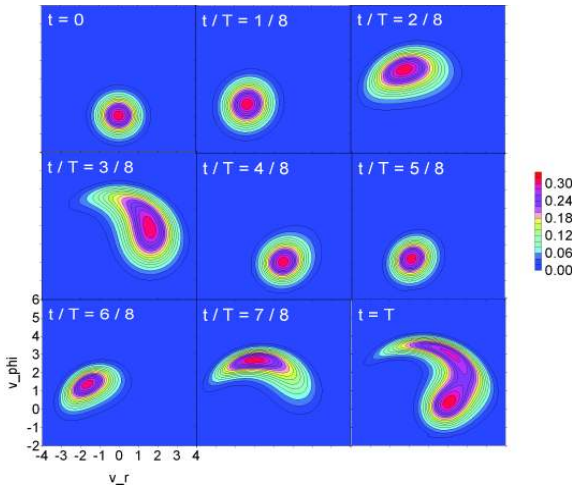

Fig. 4 Ion velocity distribution function versus time at $r = R_c$ and at $E_c/B = 2$ for $E_r = -E_c(r/R_c)e^{-0.1(r/R_c)^3}$. In all panels, $T = 2\pi/\Omega_i$.

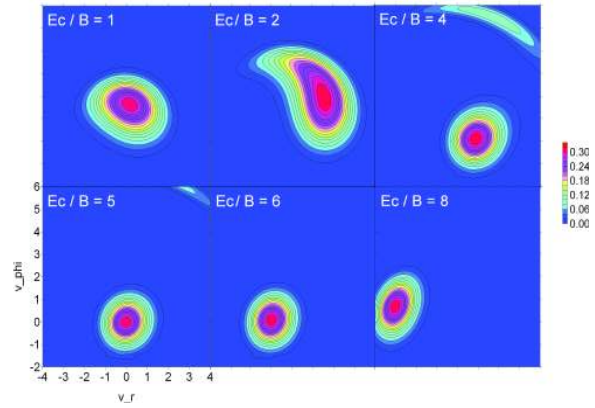

Fig. 5 Ion velocity distribution function versus E_c at $r = R_c$ and at $t = 3T/8$ (where $T = 2\pi/\Omega_i$) for $E_r = -E_c(r/R_c)e^{-0.1(r/R_c)^3}$. The halo is flying away from the core distribution. In an enlarged figure given by Fig.9 below, the center of the halo is at $v_r = 1$ and $v_\phi = 7.3$ for $E_c/B = 6$.

sharper drop in the electric field strength, which leads to fewer energetic ions in the tail to be deflected away by the $\mathbf{E} \times \mathbf{B}$ drift from the region of interest.

At this point, we would like to show another interesting feature the ion velocity distribution function reveals: a core-halo shaped appearance. This unexpected shape originates from the application of stronger electric field strengths, as shown in Fig.5. With an increasing electric field, the ion distribution function first moves in velocity space as a whole. But at $E_c/B = 4$, the teardrop-shaped distribution is separated into two parts: a core continuing to move downward, and a halo peeling off but moving upward. Different from the core-tail case, this core-halo distribution is directly related to the formation of an energetic ion beam. If the electric field continues to increase, the halo flies away from its parental core as shown in panel $E_c/B = 5$. Noticeably, the core shrinks to a smaller size than before giving off the halo. In an enlarged figure given by Fig.9 below, numerical calculations show that the center of the halo is at $v_r = 1$ and $v_\phi = 7.3$.

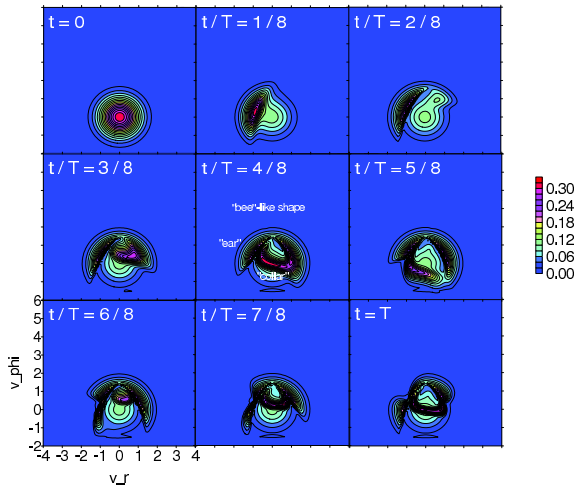

Fig. 6 Ion velocity distribution function versus time at $r = R_c$ and at $E_c/B = 2$ for $E_r = -E_c e^{-(r/R_c-1)^2/0.1^2}$: panels for time $t = 0 - T$. In all panels, $T = 2\pi/\Omega_i$. In the central panel, " 'bee-like' shape", "ear", "collar" are labeled.

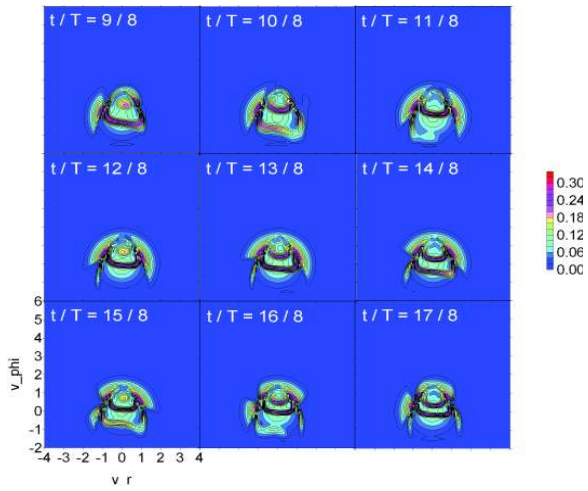

Fig. 7 Ion velocity distribution function versus time at $r = R_c$ and at $E_c/B = 2$ for $E_r = -E_c e^{-(r/R_c-1)^2/0.1^2}$: panels for time $t = T - 2T$. In all panels, $T = 2\pi/\Omega_i$.

4.3 Case 3: Sharp changes in E versus r

We intentionally choose $r = R_c$ as the layer (or surface) where space charges produce a δ-function-like radial electric field. Both inside and outside the layer, the electric field drops to zero abruptly (Curve 4 in Fig.1).

This kind of electric field structure brings about a few bizarre features to the ion velocity distribution function. First of all, at any time, the distributions are completely deformed in shape from the initial Maxwellian. However, generally speaking, the incomplete "bee"-shaped body is staying still at the initial position in velocity space, though some parts of the body move in time. An associated feature is that though there exists the strong electric field at $r = R_c$, no GC motion related to the $\mathbf{E} \times \mathbf{B}$ drift is seen to be triggered as happened in Cases 1 and 2. Both Figs.6 and 7 confirms this static evolution of the distribution function in time, respectively. Finally, an ear-collar shaped distribution is evolving on the bee-shaped body. At panel $t/T = 1/8$ in Fig.6, a bigger LHS ear first develops. This ear extends

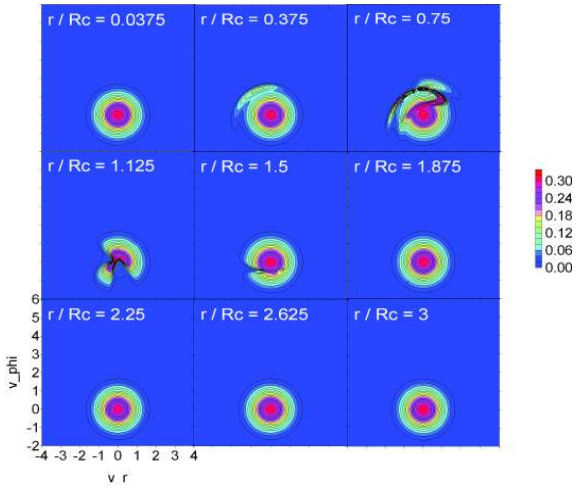

Fig. 8 Ion velocity distribution function versus radial position at $t = 7T/8$ (where $T = 2\pi/\Omega_i$) and at $E_c/B = 2$ for $E_r = -E_c e^{-(r/R_c-1)^2/0.1^2}$.

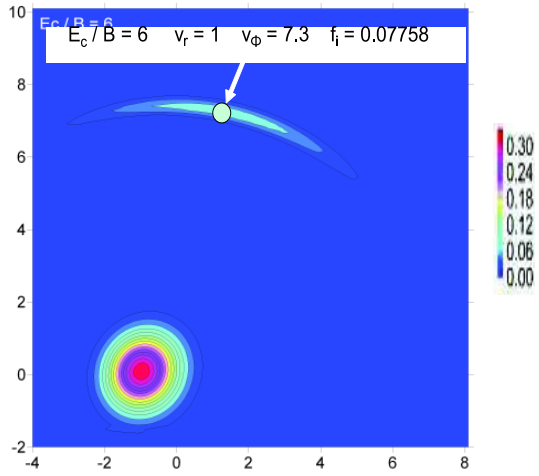

Fig. 9 Core-halo distribution function and its peak at $E_c/B = 6$ (in units of v_{th}) at $r = R_c$ and at $t = 3T/8$ (where $T = 2\pi/\Omega_i$) under the electric field structure $E_r = -E_c(r/R_c) \cdot e^{-0.1(r/R_c)^3}$.

wider in velocity space and then moves up to the top to meet with another smaller RHS ear which is also moving up from another side. At the same time, a collar is formed and moves downward while the ears move up. Fig.7 depicts this process more clearly.

At this stage, it is intriguing to know the dependence of the ion velocity distribution function on the radial position. From the profile of the electric field structure, $E_r = -E_c \exp[-(r/R_c - 1)^2/0.1^2]$, we know that the field strength decreases to zero if r deviates far away from R_c. So, at both small or large r/R_c, there is no electric field locally to drive ions. Thus, either inside or outside the cylinder the ion distribution function should keep its initial Maxwellian form. Luckily, Fig.8 reveals this feature: from panel $r/R_c = 0.0375$ to $r/R_c = 0.375$, we can see that the distribution functions are mainly Maxwellian at smaller radius. However, closer to $r/R_c = 1$, the ear-collar bee-shaped distribution is emerging from the Maxwellian till panel $r/R_c = 1.5$. After that, at larger radius the distribution returns to Maxwellian again.

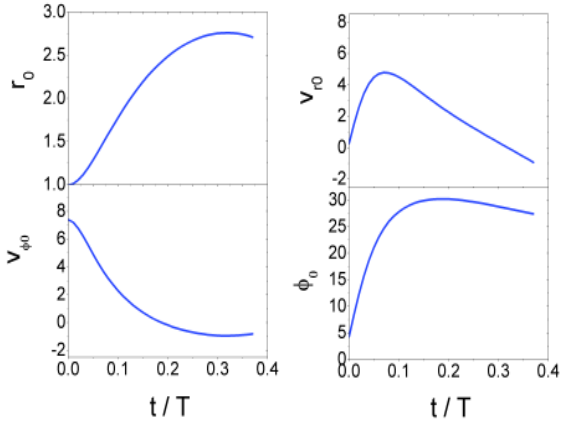

Fig. 10 Ion parameter spectra in phase space resulting in a halo distribution peak of $f_{i10} = 0.07758$ at $r = R_c$ and at $t = 3T/8$ (where $T = 2\pi/\Omega_i$) under the electric field structure used in Fig.9 for $v_r = 1$ and $v_\phi = 7.3$.

5 Backmapping phase-space parameters

In case 2, a core-halo distribution function has been found under $E_c/B \geq 4$. The ions in the halo are more energetic with a much larger drift speeds. For example, at $E_c/B = 6$, $t/T = 3/8$, numerical calculations show that the center of the halo is at $v_r = 1$ and $v_\phi = 7.3$ in velocity space at the radial position $r = R_c$. This gives a perpendicular speed $v_\perp = \sqrt{v_r^2 + v_\phi^2} \sim \sqrt{54}$ which is 5.2 times the initial perpendicular speed. Accordingly, the perpendicular ion energy has increased to 27 times of the initial energy.

The origin of these energetic ions has been found by using a back-tracing approach. By picking up a halo point in velocity space and then using the $\{v_r, v_\phi\}$ values as the initial conditions in the back-mapping equation of motion, we can immediately obtain $\{r_0, v_{r0}, v_{\phi 0}, \phi_0\}$ in phase space. Let's use the above velocity point $\{v_r = 1, v_\phi = 7.3\}$ in the halo as an example, at which the halo distribution function is maximal, $f_{i10} = 0.07758$ as shown in Fig.9. The numerical results are shown in Fig.10: this maximum halo distribution has contributions from all the ions with initial phase-space values designated by the curves from $t = 0$ to $t = 3T/8$, respectively.

6 Transport properties

Various transport properties (density, average speeds, temperatures, heat flows, etc.) are numerically calculated from velocity moments of the ion velocity distributions. For a direct comparison, Fig.11 shows these bulk parameters under the first two nonlinear electric field structures.

The evolution of these parameters in time reveals a quasi-periodic feature under either electric field structure. There is not much difference in the quasi-oscillations for the two different electric fields. However, the quasi-oscillations are not totally the same. For example, the electric field which drops more slowly outside the cylinder [electric field (1) in the figure] appears to give oscillations with higher amplitudes in density (n_i) and azimuthal components of the bulk properties (e.g., v_ϕ, T_ϕ, and q_ϕ). By contrast, the electric field which drops more quickly outside the cylinder [electric field (2) in the figure] triggers oscillations with higher amplitudes in the radial components of the bulk parameters (e.g., T_r and q_r). It deserves to be mentioned here that the existence of the heat flows indicates local temperature gradients in real space.

Under the situation of the sharp electric field case, Fig.12 shows two nine-panel plots. The upper nine panels tell us the evolution of the bulk parameters with time, while the lower nine ones show

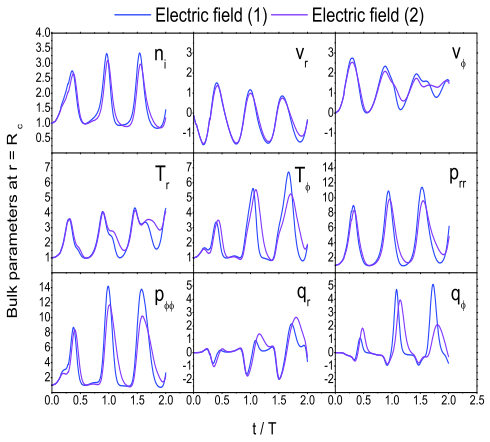

Fig. 11 Ion bulk properties as a function of time for two nonlinear electric field structures: (1) $E_r = -E_c(r/R_c)/[1+0.1(r/R_c)^3]$; (2) $E_r = -E_c(r/R_c)e^{-0.1(r/R_c)^3}$.

their changes as a function of radial position. A striking feature of the upper panels is that all bulk parameters oscillate relatively steadily with time in comparison to those under previous two electric fields. For example, they all have a time-average value plus a fluctuating component; and, the time-average values of both q_r and q_ϕ are around zero.

The lower nine panels describe that these bulk properties are localized ones. For example, outside $r = 2R_c$, they all turn out to be zero. However, in the region from $r = 0$ to $r = 2R_c$, the parameters changes violently. No doubt there are radial gradients for all of them.

7 Summary and discussion

Non-Maxwellian velocity distribution function and related observable transport parameters (e.g., bulk velocity, temperature, etc.) produced by different auroral electric field structures have been studied since the early seventies. Earlier studies had established that the ion velocity distributions under homogeneous electric fields can differ in important ways from the conventionally assumed Maxwellian (Gaussian) velocity distribution by becoming ring-shaped in velocity space under very strong electric field conditions (e.g., *Cole* 1971). By comparison to this homogeneous case, early studies had also shown that the velocity distributions under an inhomogeneous electric field which increases linearly in a specific direction in space were found to be crescent-shaped (as opposed to ring-shaped) in the velocity plane transverse to the magnetic field direction under similarly very strongly driven conditions (e.g., *St.-Maurice* & *Schunk* 1979; *St.-Maurice et al.* 1994).

However, the aurora often breaks down into elongated filaments that are aligned with the geomagnetic field. It is natural to infer from this that when important structures are found in the electrostatic fields they, too, will follow a cylindrical geometry. Our work has been oriented towards these types of ionospheric electric field structures. Our first study (Paper 1) acts as the basis of the present study, where we had assumed a simple electric field structure which is "constant" in time, but proportional to the radius, i.e., a "radially linear" electric field in space. In addition, the initial ion density was assumed "uniform" in space, and we considered collision-free conditions which are valid above 500 km in altitudes. After removal of the "radially linear" constraint from the electric field structures, we solved numerically the problem of an electric field that could follow any radially "nonlinear" evolution in space. At this stage, there was no way to seek a generalized approach for complete analytical solutions. We instead developed a "backward ray-tracking" approach (i.e., tracking the ions back in time, using the

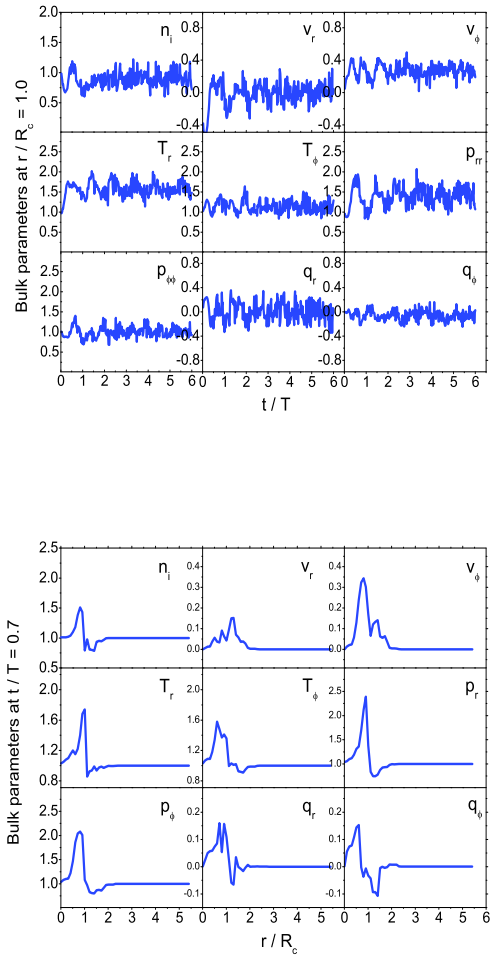

Fig. 12 Ion bulk properties under a nonlinear electric field structure $E_r = -E_c e^{-(r/R_c-1)^2/0.1^2}$. Upper 9 panels: as a function of time. Lower 9 panels: as a function of radial position.

temporal link between the initial position and velocity of an ion and the arbitrary position and velocity at any time) based on energy conservation and the equations of motion.

We verified first of all the validity of the code by reproducing all the results given in Paper 1. After that, we calculated the ion velocity distributions and bulk properties under three realistic electric field models: (1) an electric field which is proportional to the radius inside a space charge cylinder but drops off slowly out side the cylinder; (2) an electric field which is still proportional to the radius inside a space charge cylinder but drops off more quickly out side the cylinder; and, (3) an electric field which is localized at the edge of the cylinder. In regimes where the electric field dropped outside a space-charge region, the evolving velocity distribution with time was found to have many possible types of shapes, such as, deformed pancake, horseshoe, teardrop, core-halo, etc. If the electric field dropped sharply on both sides of the boundary of a region, the distribution developed an ear-collar appearance with time. Under all electric field structures, the non-Maxwellian distributions and related transport parameters were localized to the region of an electric field. In this study, we also used a backmapping technique to find where those ions contributing to a specific distribution point in velocity space came from.

In last two decades, space observations via satellites, rockets, and radars, have shown that there are numerous instances of cylindrical space-charge/electric-field arrangements in the auroral ionosphere

(such as traveling vortices, auroral rays, and lower-hybrid cavities) in different spatial and temporal scales. This motivated the present study of ions responses to electric fields in cylindrically symmetric situations. The results have made progress toward a better understanding of the physics of ion velocity distributions, transport properties, and ion oscillation mechanisms in a band around ion gyrofrequency in the auroral ionosphere under various perpendicular electric fields (**E**) crossed to the local geomagnetic field (**B**) in a cylindrical geometry.

However, though the present work offers both qualitative and quantitative insights into auroral ion distributions, as well as into their bulk properties as they are driven by different types of electric fields in auroral regions, much work is needed for more complicated situations and to explain important ionospheric phenomena measured by rockets and/or satellites. For one thing, the study should be extended to tackle an important issue in auroral physics: transverse ion energization and ion outflows in the formation of ion conics in velocity space. The first ion conic was measured by Satellite 1976-65B [*Sharp et al.* (1977)]. In that work, conic H^+ and O^+ ions were detected at about $1R_E$ in the northern dayside polar cusp. Since then, many satellites have observed ion conics in geospace [e.g., *Klumpar* (1986); *Ergun et al.* (2001); *Ergun* (2003); *McFadden et al.* (2003)]. A widely accepted process for the evolution of ion conics was described by, e.g., *Mozer* (1980); *Mozer et al.* (1980); *Gorney et al.* (1985); *Lysak* (1986); *Wu et al.* (2002): at first, some kind of mechanism has to produce transverse ion heating; heated ions are then driven upward by the geomagnetic mirror force which is proportional to the transverse kinetic energy under the conservation of the first adiabatic invariant; the total velocity of the ions takes a conic appearance at higher altitudes; the presence of parallel electric fields may contribute to a more complicated picture through "a pressure cooker" effect [*Gorney et al.* (1985); *Barakat & Barghouthi* (1994); *Wu* (2000)]. The mechanism underlying the transverse ion heating is not yet clear enough. Wave energization is one possibility, with a term to represent the perpendicular energy gain from the "wave-particle interactions (WPI)" in the conic equations [*Gorney et al.* (1985)]: $\mathrm{d}\mathcal{E}_\perp/\mathrm{d}t|_{\mathrm{WPI}}$. This term has been assumed constant (at 1 eV/s) for protons over the altitude range $0.1R_E < h < 1R_E$, and suggested to scale as $m^{\alpha-1}$ for heavy ions (α is a power-law index from the spectral fit)[*Gorney et al.* (1985); *Lund et al.* (1999)].

However, there are some problems with the WPI explanation. When taking a close look at the measurements of ion energy distributions [*Sckopke et al.* (1983); *Klumpar* (1986); *Moore et al.* (1986)], it was found that (1) a one-to-one correspondence between heated ions and any particular type of plasma waves to heat them is not obtained; (2) the energy is not always transferred from wave(s) to ions, or rather, it can flow from ions to the wave(s); and (3) the interaction of ions with small-scale potential structures (a special form of wave-particle interactions) seems closest to being responsible for the transverse ion heating. These potential structures were described as spikelets (or cavitons) [*Chang* (1993); *McFadden et al.* (1999a,b)]. However, the correlation between the ion energization and the pulsative field strengths is still open [*Schuck & Bonnell* (2003)]. We are looking forward to addressing the transverse ion energization question by employing the model employed in the paper. First of all, Paper 1 tell us that after the electric field is switched on, ions start a cyclotron oscillation (ω) about the $\mathbf{E}\times\mathbf{B}$ drift, with a temperature that changes with time. If at some point the electric field is switched off, ions will at first have the drift velocity and temperature reached just before the electric field disappears, but now the mean velocity will start to pulsate around the origin. If the electric field continues to be on and off repeatedly, ions could be heated or accelerated continuously to extraordinary levels (see St.-Maurice's original idea recorded in *Ma et al.* 2009). A related study is going on.

References

Akasofu S.-I. (1977), Physics of magnetospheric substorms, Dordrecht, Holland; Boston: D. Reidel.

Akasofu S.-I. (1981a), Energy coupling between the solar wind and the magnetosphere, *Space Sci. Rev.*, *28*(2), 121-190.

Akasofu S.-I. (1981b), The aurora: an electrical discharge phenomenon surrounding the Earth, *Rep. Prog. Phys.*, *44*(10), 1123-1149.

Alexeev I. I., Y. I. Feldstein, R. A. Greenwald (1997), Convection vortex at dayside of high latitude ionosphere, *Phys. Chem. Earth*, *22*(7-8), 691-696.

Anastasiadis A., I. A. Daglis, and C. Tsironis (2004), Ion heating in an auroral potential structure, *Astron. Astrophys.*, *419*, 793-799.
Banaszkiewicz M., and W.-H. Ip (1993), The velocity distribution functions of oxygen and sulphur ions in the Io plasma torus, *Adv. Space Res.*, *13*(10), 331-335.
Barakat A. R., and I. A. Barghouthi (1994), The effect of wave-particle interactions on the polar wind O^+, *Geophys. Res. Lett.*, *21*(21), 2279-2282.
Baranoski G. V. G., J. G. Rokne, P. Shirley, et al. (2003), Simulating the aurora, *J. Visual. Comput. Animat.*, *14*, 43-59.
Bernhardt P. A., P. J. Erickson, F. D. Lind, et al. (2005), Artificial disturbances of the ionosphere over the Millstone Hill incoherent scatter radar from dedicated burns of the space shuttle orbital maneuver subsystem engines, *J. Geophys. Res.*, *110*, A05311.
Bock B. J. J. (2005), Study of lower-hybrid cavities detected by the GEODESIC and OEDIPUS-C sounding rockets, *M.Sc. Thesis*, University of Calgary.
Burchill J. K., D. J. Knudsen, B. J. J. Bock, et al. (2004), Core ion interactions with BBELF, lower hybrid, and Alfvén waves in the high-latitude topside ionosphere, *J. Geophys. Res.*, *109*, A01219.
Chang T. (1993), Lower-hybrid collapse, caviton turbulence, and charged particle energization in the topside aurora1 ionosphere and magnetosphere, *Phys. Fluids B*, *5*(7), 2646-2656.
Cole K. D. (1971), Atmospheric excitation and ionization by ions in strong auroral and man-made electric fields, *J. Atmo. Terr. Phys.*, *33*, 1241-1249.
Cole K. D. (1976), Effects of crossed magnetic and spatially dependent electric fields on charged particles motion, *Planet. Space Sci.*, *24*, 515-518.
Cranmer S. R. (2002), Solar wind acceleration in coronal holes, in: *ESA SP-508*, Proc. of the SOHO-11 symposium: From solar minimum to solar maximum, Davos, Switzerland, 361-366.
Danielides M. A., and A. Kozlovsky (2001), Aurora vortex structures as a result of disturbed geomagnetic conditions, in *The Outer Heliosphere: The Next Frontiers*, Eds.: K. Scherer, Horst Fichtner, Hans Jörg Fahr, and Eckart Marsch, *COSPAR* Colloquiua Series, *11*, Amsterdam: Pergamon Press.
Date H., and M. Shimozuma (2001), Boltzmann equation description of electron transport in an electric field. with cylindrical or spherical symmetry, *Phys. Rev. E*, *64*, 066410.
Earle G. D., M. C. Kelley, G. Ganguli (1989), Large velocity shears and associated electrostatic waves and turbulence in the auroral F region, *J. Geophys. Res.*, *94*(1), 15,321-15,333.
Ergun R. (2003), Auroral Particle Acceleration by Strong Double Layers, *45th Annual Meeting of the Division of Plasma Physics*, *Meeting ID: DPP03*, Albuquerque, New Mexico.
Ergun R. E., Y.-J. Su, L. Andersson, et al. (2001), Direct observation of localized parallel electric fields in a space plasma, *Phys. Rev. Lett.*, *87*(4), 045003.
Frank L. A., and W. R. Paterson (2000), Return to Io by the Galileo spacecraft: plasma observations, *J. Geophys. Res.*, *105*, 25,363-25,378.
Ganguli G., Y. C. Lee, and P. J. Palmadesso (1988), Kinetic theory for electrostatic waves due to transverse velocity shears, *Phys. Fluids*, *31*(4), 823-838.
Gorney D. J., Y. T. Chiu, and D. R. Croley (1985), Trapping of ion conics by downward parallel electric fields, *J. Geophys. Res.*, *90*, A5, 4205-4210.
Huang C.-S., G. J. Sofko, K. A. McWilliams, et al. (1998), SuperDARN observations of quasi-stationary mesoscale convection vortices in the dayside high-latitude ionosphere, *J. Geophys. Res.*, *103*(A12), 29,239-29,252.
Kan J. R., and S.-I. Akasofu (1989), Electrodynamics of solar wind-magnetosphere-ionosphere interactions, *IEEE Trans. Plasma Sci.*, *17*(2), 83-108.
Klumpar D. M. (1986), A digest and comprehensive biblography on transverse auroral ion acceleration, *Geophys.Mono.*, *38*: Ion Acceleration in the Magnetosphere and Ionosphere, Eds.: Tom Chang (Editor-in-Chief), M.K. Hudson, J.R. Jasperse, R.G. Johnson, P.M. Kintner, M. Schulz (Co-Editors), AGU, Washington, D.C., 389-398.
Knudsen D. J., B. J. J. Bock, S. R. Bounds, et al. (2004), Lower-hybrid cavity density depletions as a result of transverse ion acceleration localized on the gyroradius scale, *J. Geophys. Res.*, *109*, A04212.
Lockwood M., B. J. I. Bromage, R. B. Horne, et al. (1987), Non-Maxwellian ion velocity distributions observed using EISCAT, *Geophys. Res. Lett.*, *14*, 111-114.
Lund E. J., E. Möbius, R. E. Ergun, et al. (1999), Mass-dependent effects in ion conic production: the role of parallel electric fields, *Geophys. Res. Lett.*, *26*(24), 3593-3596.
Lyon J. G. (2000), The solar wind-magnetosphere-ionosph-ere system, *Science*, *288*(16), 1987-1991.
Lysak R. L. (1986), Ion acceleration by wave-particle interaction, in: Ion acceleration in the magnetosphere and ionosphere, *AGU Geophys. Mono.*, *38*, 261-270.

Ma J. Z. G., and J.-P. St.-Maurice (2008), Ion distribution functions in cylindrically symmetric electric fields in the auroral ionosphere: The collision-free case in a uniformly charged configuration, *J. Geophys. Res.*, *113*, A05312 (Paper 1).
Ma J. Z. G., and J.-P. St.-Maurice (2014), Backward mapping solutions of the Boltzmann equation in cylindrically symmetric, uniformly charged auroral ionosphere, *Astrophys. Space Sci.*, ASTR-D-00705, 21 pages, in revision.
Ma J. Z. G., J.-P. St.-Maurice, and A. Hirose (2009), Non-wave mechanism of transverse ion heating in magnetic flux tubes, *Phys. Scr.*, *80*(2), 025501.
Marklund G., I. Sandahl, and H. Opgenoorth (1982), A study of the dynamics of a discrete auroral arc, *Planet. Space Sci.*, *30*(2), 179-197.
McFadden J. P., C. W. Carlson, and R. E. Ergun (1999a), Microstructure of the auroral acceleration region as observed by FAST, *J. Geophys. Res.*, *104*, 14,453-14,480.
McFadden J. P., C. W. Carlson, R. E. Ergun, et al. (1999b), Ion and electron characteristics in auroral density cavities associated with ion beams: No evidence for cold ionospheric plasma, *J. Geophys. Res.*, *104*(A7), 14671-14682.
McFadden J. P., C. W. Carlson, R. E. Ergun, et al. (2003), FAST observations of ion solitary waves, *J. Geophys. Res.*, *108*(A4), 8018.
Meziane K., W. Wilber, A. M. Hamza, et al. (2006), Upstream field-aligned beams: results from Cluster, in: *ESA SP-598*, Proc. of Cluster and Double Star symposium, 5th Anniversary of Cluster in Space, Noordwijk, Netherlands, 1-5.
Moore T. E., J. H. Waite (Jr.), M. Lockwood, et al. (1986), Observations of coherent transverse ion acceleration, *Geophys.Mono.*, *38*: Ion Acceleration in the Magnetosphere and Ionosphere, Eds.: Tom Chang (Editor-in-Chief), M. K. Hudson, J. R. Jasperse, R. G. Johnson, P. M. Kintner, M. Schulz (Co-Editors), AGU, Washington, D.C., 50-55.
Moore T. E., M. O. Chandler, C. J. Pollock, et al. (1996), Plasma heating and flow in an auroral arc, *J. Geophys. Res.*, *101*(A3), 5279-5298.
Mozer F. S. (1980), On the lowest-altitude S3-3 observations of electrostatic shocks and parallel electric fields, *Geophys. Res. Lett.*, *7*, 1097-1098.
Mozer F., C. Cattell, R. Lysak, et al. (1980), Satellite measurements and theories of low altitude auroral particle acceleration, *Space Sci. Rev.*, *27*, 155-213.
Ott E., and D. T. Farley (1975), Microinstabilities and the production of short-wavelength irregularities in the auroral F region, *J. Geophys. Res.*, *80*, 4599-4602.
Pietrowski D., K. A. Lynch, R. B. Torbert, et al. (1999), Multipoint measurements of large DC electric fields and shears in the auroral zone, *Geophys. Res. Lett.*, *26*(22), 3369-3372.
Raman R. S. V. (1980), Incoherent scattering of radar waves in the auroral ionosphere, *Ph.D. thesis*, University of Michigan.
Raman R. S. V., J.-P. St.-Maurice, and R. S. B. Ong (1981), Incoherent scattering of radar waves in the auroral ionosphere, *J. Geophys. Res.*, *86*, 4751-4762.
Roig F. S., and J. E. Schoutens (1986), Remarks on the use of Boltzmann's equation for electrical conduction calculations in metal matrix and in situ composites, *J. Mater. Sci.*, *21*, 2767-2770.
Rothwell P. L., Silevitch M. B., L. P. Block, et al. (1992), Acceleration and stochastic heating of ions drifting through an auroral arc, *J. Geophys. Res.*, *97*, 19,333-19,339.
Rothwell P. L., M. B. Silevitch, L. P. Block, et al. (1995), Particle dynamics in a spatially varying electric field, *J. Geophys. Res.*, *100*, 14,875-14,886.
Schuck P. W., and J. W. Bonnell (2003), Ray trajectories of lower hybrid solitary structures, *J. Geophys. Res.*, *108*(A5), 1175.
Schuck P. W., J. W. Bonnell, and P. M. Kintner (Jr.) (2003), A review of lower hybrid solitary structures, *IEEE Trans. Plasma Sci.*, *31*, 1125-1177.
Schunk R. W., and J. C. G. Walker (1972), Ion velocity distributions in the auroral ionosphere, *Planet. Space Sci.*, *20*, 2175-2191.
Sckopke N., G. Paschmann, S. J. Bame, et al. (1983), Evolution of ion distributions across the nearly perpendicular bow shock–Specularly and non-specularly reflected-gyrating ions, *J. Geophys. Res.*, *88*, 6121-6136.
Sharp R. D., R. G. Johnson, and E. G. Shelley (1977), Observations of an ionospheric acceleration mechanism procucing energetic (keV) ions primarily normal to the geomagnetic field direction, *J. Geophys. Res.*, *82*, 3324-3328.
Steffl A. J. (2005), The Io plasma torus during the Cassini encounter with Jupiter: temporal, radial and azimuthal variations, *Ph.D. thesis*, University of Colorado.

St.-Maurice J.-P., and R. W. Schunk (1973), Auroral ion velocity distributions using a relaxation model, *Planet. Space Sci.*, *21*, 1115-1130.
St.-Maurice J.-P., and R. W. Schunk (1974), Behavior of ion velocity distributions for a simple collision model, *Planet. Space Sci.*, *21*, 1-18.
St.-Maurice J.-P., W. B. Hanson, and J. C. G. Walker (1976), Retarding potential analyzer measurement of the effect of ion-neutral collisions on the ion velocity distribution in the auroral ionosphere, *J. Geophys. Res.*, *81*(31), 5438-5446.
St.-Maurice J.-P. (1978), On a mechanism for the formation of VLF electrostatic emissions in the high latitude F region, *Planet. Space Sci.*, *26*, 801-816.
St.-Maurice J.-P., and R. W. Schunk (1979), Ion velocity distributions in the high latitude ionosphere, *Rev. Geophys. and Space Phys.*, *17*, 99-134.
St.-Maurice J.-P., E. Winkler, and A. M. Hamza (1994), Ionospheric ion velocity distributions and associated transport properties in the presence of auroral electric field gradients, *J. Geophys. Res.*, *99*, 19,527-19,548.
Swift D. W. (1975), The effect of electric fields and ion-neutral collisions on Thomson scatter spectra, *J. Geophys. Res.*, *80*(1), 4380-4382.
Takahashi T., K. Morohashi, N. Iwasawa, et al. (2004), Kinetic simulation for infinitely long cylindrical high-beta plasma with field-null surface, *J. Plasma Fusion Res. Series*, *6*, 485-488.
Vandenplas P. E., and R. W. Gould (1964), Equations of a hot inhomogeneous plasma model-I: resonance frequencies of a cylindrical plasma column, *Plasma Phys. (J. Nucl. Energy Part C)*, *6*, 449-458.
Vogelsang H., H. Lühr, H. Voelker, et al. (1993), An ionospheric travelling convection vortex event observed by ground-based magnetometers and by VIKING, *Geophys. Res. Lett.*, *20*, 2343-2346.
Whealton J. H., and S.-B. Woo (1971), Ion velocity distribution of a weakly ionized gas in a uniform electric field of arbitrary strength, *Phys. Res. A*, *6*(6), 2319-2325.
Wu X.-Y. (2000), Auroral ionospheric ion upflows and outflows: Satellite observations and dynamic fluid-kinetic simulations, *Ph.D. thesis*, University of Alabama (Hunts-ville).
Wu X.-Y., J. L. Horwitz, and J.-N. Tu (2002), Dynamic fluid kinetic (DyFK) simulation of auroral ion transport: Synergistic effects of parallel potentials, transverse ion heating, and soft electron precipitation, *J. Geophys. Res.*, *107*(A10), 1283.
Yau A. W., W. B. Whalen, W. K. Peterson, et al. (1984), Distribution of upflowing ionospheric ions in the high-altitude polar cap and auroral ionosphere, *J. Geophys. Res.*, *89*, 5507-5522.
Yermolaev I., A. O. Fedorov, O. L. Vaisberg, et al. (1997), Ion distribution dynamics near the Earth's bow shock: first measurements with the 2D ion energy spectrometer CORALL on the INTERBALL/Tail-probe satellite, *Ann. Geophys.*, *15*(5), 533-541.